ACTA MECHANICA SOLIDA SINICA 30 (2017) 39–50

Available online at www.sciencedirect.com

ScienceDirect

journal homepage: www.elsevier.com/locate/CAMSS

Interaction between a screw dislocation and a circular nano-inhomogeneity with a bimaterial interface

Tengwu He, Wanshen Xiao, Xiangdong Li, Yan Zhang*

College of Mechanical and Vehicle Engineering, Hunan University, Changsha, Hunan Province 410082, PR China

ARTICLE INFO

Article history:
Received 22 January 2016
Revised 13 August 2016
Accepted 29 August 2016
Available online 16 February 2017

Keywords:
Screw dislocation
Image force
Conformal mapping
Bimaterial interface
Nano-inhomogeneity

ABSTRACT

The problem of a screw dislocation interacting with a circular nano-inhomogeneity near a bimaterial interface is investigated. The stress boundary condition at the interface between the inhomogeneity and the matrix is modified by incorporating surface/interface stress. The analytical solutions to the problem in explicit series are obtained by an efficient complex variable method associated with the conformal mapping function. The image force exerted on the screw dislocation is also derived using the generalized Peach–Koehler formula. The results indicate that the elastic interference of the screw dislocation and the nano-inhomogeneity is strongly affected by a combination of material elastic dissimilarity, the radius of the inclusion, the distance from the center of inclusion to the bimaterial interface, and the surface/interface stress between the inclusion and the matrix. Additionally, it is found that when the inclusion and Material 3 are both harder than the matrix ($\mu_1 > \mu_2$ and $\mu_3 > \mu_2$), a new stable equilibrium position for the screw dislocation in the matrix appears near the bimaterial interface; when the inclusion and Material 3 are both softer than the matrix ($\mu_1 < \mu_2$ and $\mu_3 < \mu_2$), a new unstable equilibrium position exists close to the bimaterial interface.

1. Introduction

Nanocomposite solids with special physical properties (high strength, high toughness, high heat, high conductivity, etc.) serve as key materials and are widely used in high technological fields. For the purpose of acquiring better performance of nanomaterials, it is essential to study the interaction between nanoscale structure and crystal lattice defects such as dislocations, disclinations and twins in detail. Its effect plays an extremely great part in the material stability, physical and mechanical performance—strength and plastic deformation. In view of their importance, a great number of contributions have been conducted toward the problem concerning materials science, solid state physics and nanomechanics during the last several decades [1–7].

For a nanoscale inclusion embedded in a matrix, the interface condition in researching the mechanical behavior of the matrix is an important factor. To our knowledge, when the size of inclusion is reduced to nanometer scale, atoms at the surface/interface possess their own unique environment and differ from the atoms in the surrounding material. As a result of the equilibrium lattice spacing at the surface/interface, the surface/interface stress emerges, which needs to be taken into consideration [8]. Gurtin and his coworkers [9,10] firstly presented a classical continuum model for the surface/interface stress problems on elastic solid. At

* Corresponding author.
E-mail address: xwshndc@126.com (Wanshen Xiao).

http://dx.doi.org/10.1016/j.camss.2016.08.001

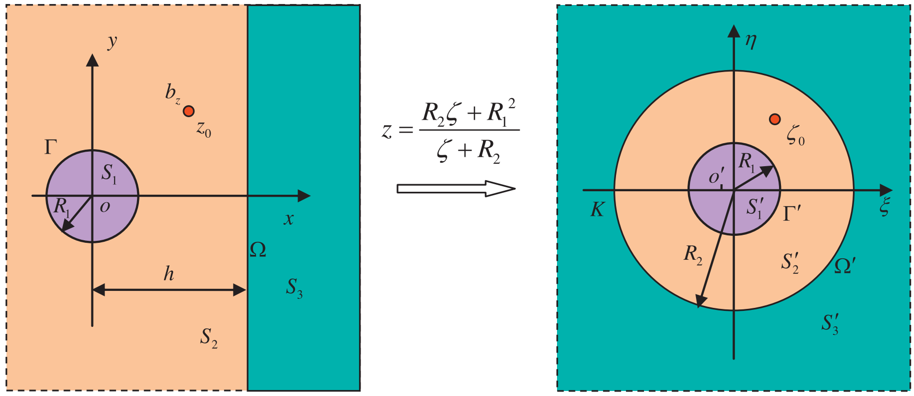

Fig. 1 – (a) Schematic diagram of a screw dislocation. (b) The ζ-plane after conformal mapping in the current nanocomposite model.

present, the surface/interface stress model has been widely employed to theoretically describe some unusual behavior related to the interface stress in nanomaterials [11–17].

The interaction between a dislocation and a nano-inclusion is an important topic in studying the mechanical behavior of materials. Based on the above-mentioned surface/interface stress model, Fang and Liu [18–20] dealt with the elastic interaction between a screw dislocation and a circular nano-inhomogeneity or a nano-hole with interface stress. Gutkin et al. [21] considered the elastic behavior of an edge dislocation located in the shell of nanowire by applying the theory of surface/interface elasticity. Tian [22] investigated the elastic field with a nanoscale elliptical inhomogeneity embedded in an infinite matrix under far-field loading and a uniform eigenstrain. Subsequently, the problem of a dislocation interacting with an elliptical nano-inhomogeneity is carried out by Luo [23,24] with different kinds of dislocations. Li [25] examined the elastic interaction between a screw dislocation and a nanoscale cylindrical inclusion in a half-plane.

The references mentioned above are mainly focused on two-phase materials. Nevertheless, most materials for engineering application consist of multiphase systems. Fortunately, Christensen and Lo [26] introduced a reasonably simplified three-phase model consisting of three concentric regions to describe the behavior of these interactions. Applying the simplified three-phase model, the exact solution for the stress field with an edge dislocation located in a three-phase composite cylinder was then derived by Luo and Chen [27]. Later on, Xiao and Chen [28] analyzed the problem for elastic interaction between a screw dislocation and nearby inclusions in a fiber-reinforced composite material. In addition, plenty of investigations have been conducted based on the three-phase model [29–32].

However, composite materials with multiphase systems are in general combined with different shapes, sizes and other styles. The elastic interaction between a screw dislocation and a circular inhomogeneity with a bimaterial interface and interface stress has not been studied. In the present paper, we address the elastic interaction between a screw dislocation and a circular inhomogeneity with interface stress near a bimaterial interface by using the conformal mapping technique. The surface/interface stress model is utilized at the interface between the inhomogeneity and the matrix. The explicit solutions of image force acting on the screw dislocation located in Material 2 and Material 3 are calculated using the Peach–Koehler formula. The stability of a screw dislocation located in Material 2 with interface stress is evaluated in detail. Finally, the influence of variable parameters (interface stress and material mismatch) on the image force is examined by several numerical examples.

2. Basic formulations

There is a nano-inclusion (Material 1) near a bimaterial interface, as shown in Fig. 1, where R_1 and h are the inclusion radius and the distance between the center of inclusion and the bimaterial interface, respectively. Material 2 and Material 3 occupy the regions denoted by S_2 and S_3, respectively. The inclusion, with its center at the origin of the Cartesian coordinate system, occupies a region denoted by S_1, and the bimaterial interface is perpendicular to the x-axis. The shear moduli of S_1, S_2, and S_3 are respectively μ_1, μ_2, and μ_3. "Γ" and "Ω" represent the Material 2/inhomogeneity interface and the bimaterial interface, respectively. It is assumed that Material 2, Material 3 and the nano-inhomogeneity are all homogeneous and isotropic.

For the convenience of analysis, the following conformal mapping function is adopted [33,34]

$$z = \omega(\zeta) = \frac{R_2\zeta + R_1{}^2}{\zeta + R_2} \tag{1}$$

where $R_2 = h + \sqrt{h^2 - R_1{}^2}$ and $z = x + iy$, $\zeta = \xi + i\eta$. Utilizing the mapping function, regions of S_1, S_2 and S_3 in the z-plane are transformed onto the domain $S'_1(|\zeta| < R_1)$,$S'_2(R_1 < |\zeta| < R_2)$, and $S'_3(|\zeta| > R_2)$ in the ζ-plane correspondingly. The coordinate origin o, the point at infinity and z_0 in the z-plane are mapped to $o'(\zeta = -R_1{}^2/R_2)$, $K(\zeta = -R_2)$ and ζ_0 in the ζ-plane, as depicted in Fig. 1(b).

For the current anti-plane problem, the constitutive equations of displacement and stress are presented as follows [9,35]

$$\frac{\partial^2 w_j}{\partial x^2}+\frac{\partial^2 w_j}{\partial y^2}=0 \tag{2}$$

$$\tau_{rzj}=2\mu_j\varepsilon_{rzj},\ \tau_{\theta zj}=2\mu_j\varepsilon_{\theta zj} \tag{3}$$

where w_j (j=1, 2, 3) refers to the anti-plane displacements in nano-inhomogeneity, Material 2 and Material 3, respectively; μ_j are shear moduli, and τ_{rzj} (ε_{rzj}) and $\tau_{\theta zj}$ ($\varepsilon_{\theta zj}$) are the stress (strain) components in polar coordinates system (r, θ). Nevertheless, the interface showing interface stress owns its intrinsic constants and is expressed by a new constitutive equation as below [11,29,36,37]

$$\tau^{\Gamma}_{\theta z}=2(\mu^{\Gamma}-\tau^{\Gamma})\varepsilon^{\Gamma}_{\theta z},\ [\tau_{rz}(t)]=\frac{1}{R}\frac{\partial\tau^{\Gamma}_{\theta z}}{\partial\theta} \tag{4}$$

where the superscript "Γ" denotes the interface between Material 2 and the inhomogeneity, $\tau^{\Gamma}_{\theta z}$ and $\varepsilon^{\Gamma}_{\theta z}$ are the interface stress and strain components, μ^{Γ} is the interfacial/face elastic constant, τ^{Γ} denotes the residual interface/face tension, and $t=Re^{i\theta}$ refers the points on the circular interface Γ. Besides, $[\tau_{rz}(t)]$ represents the discontinuity of the stress across the interface Γ.

For a coherent interface, the interfacial strain $\varepsilon^{\Gamma}_{\theta z}$ is equal to the associated tangential strain abutting the bulk materials. For semi-coherent or incoherent interfaces, additional conditions in the interfacial strain are required. The case for a coherent interface will be considered in what follows.

Allowing for the relation of $\varepsilon^{\Gamma}_{\theta z}(t)=\varepsilon_{\theta z}(t)$, then combining Eqs. (3) and (4), we can get

$$[\tau_{rz}(t)]=\frac{(\mu^{\Gamma}-\tau^{\Gamma})}{R\mu}\frac{\partial\tau_{\theta z}(t)}{\partial\theta} \tag{5}$$

With the help of Eqs. (1)–(5), the boundary conditions at different interfaces can be obtained as follows

$$w_1(z_\Gamma)=w_2(z_\Gamma),\ \tau_{rz2}(z_\Gamma)-\tau_{rz1}(z_\Gamma)=\frac{\mu^{\Gamma}-\tau^{\Gamma}}{R_1\mu_2}\frac{\partial\tau_{\theta z2}(z_\Gamma)}{\partial\theta},\ z_\Gamma\in\Gamma \tag{6}$$

$$w_2(z_\Omega)=w_3(z_\Omega),\quad \tau_{rz2}(z_\Omega)=\tau_{rz3}(z_\Omega),\quad z_\Omega\in\Omega \tag{7}$$

where the subscripts "1", "2" and "3" denote regions of the inclusion, Material 2 and Material 3, respectively, and z_Γ and z_Ω denote the points at the Γ interface and at the Ω interface, respectively.

For anti-plane problems, the displacement w, shear stresses τ_{rz} and $\tau_{\theta z}$ can be given in terms of an analytical function $f(z)$ of the complex variable $z=x+iy$ as follows:

$$w=[f(z)+\overline{f(z)}]/2 \tag{8}$$

$$\tau_{rz}-i\tau_{\theta z}=\mu e^{i\alpha}f'(z) \tag{9}$$

where μ is shear modulus of the material, the "–" shows the complex conjugate, and $f'(z)$ denotes the differentiation with respect to the argument z.

The next step is to calculate the complex potentials $f_1(z)$, $f_2(z)$, and $f_3(z)$ in the inclusion, Material 2 and Material 3 with the aid of Eqs. (6)–(9), respectively.

2.1. *A screw dislocation in Material 2*

Considering a screw dislocation with the Burgers vector $b(0, 0, b_z)$, which is assumed to be straight and infinite along the direction perpendicular to the x–y plane and is located at an arbitrary point $z_0=x_0+iy_0$ in Material 2, the complex potential in the Material 2 region can be written in the following form [38,39]

$$f_1(z)=f_{10}(z),\ z\in S_1 \tag{10}$$

$$f_2(z)=\frac{b_z}{2\pi i}\ln(z-z_0)+f_{20}(z),\ z\in S_2 \tag{11}$$

where $f_{20}(z)$ is analytical in the region of S_2. Ignoring the constant terms representing the rigid body displacement and taking into account Eq. (1), Eqs. (10) and (11) can lead to

$$f_1(\zeta)=f_{10}(\zeta),\ |\zeta|<R_1 \tag{12}$$

$$f_2(\zeta)=\frac{b_z}{2\pi i}[\ln(\zeta-\zeta_0)-\ln(\zeta+R_2)]+\sum_{k=0}^{\infty}a_k\zeta^{-k-1}+\sum_{k=0}^{\infty}b_k\zeta^{k+1},\quad R_1<|\zeta|<R_2 \tag{13}$$

where $\zeta_0=(R_2z_0-R_1^2)/(R_2-z_0)$.

In order to solve the current problem more easily, the following new auxiliary functions are recommended in the corresponding regions based on the Schwarz symmetry principle.

$$F_2(\zeta)=\zeta f'_2(\zeta)=\frac{b_z}{2\pi i}\left(\frac{\zeta}{\zeta-\zeta_0}-\frac{\zeta}{\zeta+R_2}\right)-\sum_{k=0}^{\infty}a_k(k+1)\zeta^{-k-1}+\sum_{k=0}^{\infty}b_k(k+1)\zeta^{k+1},\quad R_1<|\zeta|<R_2 \tag{14}$$

$$F_2{}^*(\zeta)=\overline{F_2}(R_1{}^2/\zeta)=\frac{b_z}{2\pi i}\left(\frac{\zeta}{\zeta-\zeta_1{}^*}-\frac{\zeta}{\zeta+\zeta_2{}^*}\right)-\sum_{k=0}^{\infty}\overline{a_k}(k+1)\frac{\zeta^{k+1}}{R_1{}^{2k+2}}+\sum_{k=0}^{\infty}\overline{b_k}(k+1)\frac{R_1{}^{2k+2}}{\zeta^{k+1}},\quad \frac{R_1{}^2}{R_2}<|\zeta|<R_1 \tag{15}$$

$$F_2{}^{**}(\zeta)=\overline{F_2}(R_2{}^2/\zeta)=\frac{b_z}{2\pi i}\left(\frac{\zeta}{\zeta-\zeta_2{}^{**}}-\frac{\zeta}{\zeta+R_2}\right)-\sum_{k=0}^{\infty}\overline{a_k}(k+1)\frac{\zeta^{k+1}}{R_2{}^{2k+2}}+\sum_{k=0}^{\infty}\overline{b_k}(k+1)\frac{R_2{}^{2k+2}}{\zeta^{k+1}},\quad R_2<|\zeta|<\frac{R_2{}^2}{R_1} \tag{16}$$

where $\zeta_1{}^*=R_1{}^2/\overline{\zeta_0}$, $\zeta_2{}^*=R_1{}^2/R_2$ and $\zeta_2{}^{**}=R_2{}^2/\overline{\zeta_0}$.

On the basis of the equilibrium condition at the interface Ω between Material 2 and Material 3, the analytical function $F_3(\zeta)$ in the Material 3 region is given by

$$F_3(\zeta)=\zeta f'_3(\zeta)=\frac{b_z}{2\pi i}+F_{30}(\zeta),\ |\zeta|>R_2 \tag{17}$$

where $F_{30}(\zeta)$ is an analytical function in the Material 3 region.

In view of Eq. (17), we have

$$F_3{}^*(\zeta)=\overline{F_3}(R_2{}^2/\zeta)=-\frac{b_z}{2\pi i}+F_{30}{}^*(\zeta),\ |\zeta|<R_2 \tag{18}$$

According to Eq. (9), the following expressions can be obtained

$$\begin{aligned}\sigma_{rz}&=\frac{\mu e^{i\alpha}f'(z)+\mu e^{-i\alpha}\overline{f'(z)}}{2}\\ \sigma_{\theta z}&=-\frac{\mu e^{i\alpha}f'(z)-\mu e^{-i\alpha}\overline{f'(z)}}{2i}\end{aligned} \tag{19}$$

where $f'(z)=f'(\zeta)/\omega'(\zeta)$.

Following England [40], Tian and Rajapakse [22], we have

$$e^{i\alpha}=\frac{\zeta\omega'(\zeta)}{|\zeta\omega'(\zeta)|},\quad e^{-i\alpha}=\frac{\overline{\zeta\omega'(\zeta)}}{|\zeta\omega'(\zeta)|} \tag{20}$$

The partial differentiation of the tangential direction α in Eq. (6) can be written as

$$\frac{\partial\Delta}{\partial\theta}=\frac{\partial\Delta}{\partial\zeta}\frac{\partial\zeta}{\partial z}\frac{\partial z}{\partial\theta}+\frac{\partial\Delta}{\partial\bar\zeta}\frac{\partial\bar\zeta}{\partial\bar z}\frac{\partial\bar z}{\partial\theta},\quad\frac{\partial z}{\partial\theta}=ie^{i\alpha},\quad\frac{\partial\bar z}{\partial\theta}=-ie^{-i\alpha} \tag{21}$$

where $\Delta=\frac{\zeta f'_2(\zeta)-\overline{\zeta f'_2(\zeta)}}{|\zeta\omega'(\zeta)|}$.

From Eqs. (19)–(21), the displacement and stress boundary conditions in Eq. (6) can be obtained as

$$[F_1(t)+F_2{}^*(t)]^{(1)}=[F_2(t)+F_1{}^*(t)]^{(2)},\quad |t|=R_1 \tag{22}$$

$$\begin{aligned}&[\mu_1F_1(t)-(\mu_2+M)F_2{}^*(t)-NtF'_{2*}(t)]^{(1)}\\&=[(\mu_2-M)F_2(t)-\mu_1F_1{}^*(t)-NtF'_2(t)]^{(2)},\ |t|=R_1\end{aligned} \tag{23}$$

where $N=(\mu^\Gamma-\tau^\Gamma)(R_1{}^2+R_2{}^2+2R_1R_2\cos\alpha)/[R_1{}^2(R_2{}^2-R_1{}^2)]$, $M=4i\sin\alpha(\mu^\Gamma-\tau^\Gamma)R_2/[R_1(R_2{}^2-R_1{}^2)]$, the superscripts (1), (2), and (3) refer to the boundary values as approached from the respective regions occupied by Material 1, Material 2 and Material 3, respectively.

Combining Eq. (14) with Eq. (15), and according to the generalized Liouville theorem [35], Eqs. (22) and (23) result in

$$g(\zeta)=\begin{cases}F_1(\zeta)+F_2{}^*(\zeta), & \frac{R_1{}^2}{R_2}<|\zeta|<R_1\\ F_2(\zeta)+F_1{}^*(\zeta), & R_1<|\zeta|<R_2\end{cases} \tag{24}$$

$$h(\zeta)=\begin{cases}\mu_1F_1(\zeta)-(\mu_2+M)F_2{}^*(\zeta)-\zeta NF'_{2*}(\zeta), & \frac{R_1{}^2}{R_2}<|\zeta|<R_1\\ (\mu_2-M)F_2(\zeta)-\mu_1F_1{}^*(\zeta)-\zeta NF'_2(\zeta), & R_1<|\zeta|<R_2\end{cases} \tag{25}$$

where

$$\begin{aligned}g(\zeta)=&\frac{b_z}{2\pi i}\left(\frac{\zeta}{\zeta-\zeta_0}-\frac{\zeta}{\zeta+R_2}\right)+\frac{b_z}{2\pi i}\left(\frac{\zeta}{\zeta-\zeta_1{}^*}-\frac{\zeta}{\zeta+\zeta_2{}^*}\right)\\&+\sum_{k=0}^{\infty}b_k(k+1)\zeta^{k+1}+\sum_{k=0}^{\infty}\overline{b_k}(k+1)\frac{R_1{}^{2k+2}}{\zeta^{k+1}}\end{aligned} \tag{26}$$

$$\begin{aligned}h(\zeta)=&(\mu_2-M+N)\frac{b_z}{2\pi i}\left(\frac{\zeta}{\zeta-\zeta_0}-\frac{\zeta}{\zeta+R_2}\right)\\&+(\mu_2-M-N(k+1))\sum_{k=0}^{\infty}b_k(k+1)\zeta^{k+1}\\&-(\mu_2+M-J_2)\frac{b_z}{2\pi i}\left(\frac{\zeta}{\zeta-\zeta_1{}^*}-\frac{\zeta}{\zeta+\zeta_2{}^*}\right)\\&-(\mu_2+M-N(k+1))\sum_{k=0}^{\infty}\overline{b_k}(k+1)\frac{R_1{}^{2k+2}}{\zeta^{k+1}}\\&+N\frac{b_z}{2\pi i}\left[\frac{\zeta_0{}^2}{(\zeta-\zeta_0)^2}-\frac{R_2{}^2}{(\zeta+R_2)^2}+\frac{\zeta_1{}^{*2}}{(\zeta-\zeta_1{}^*)^2}-\frac{\zeta_2{}^{*2}}{(\zeta+\zeta_2{}^*)^2}\right]\end{aligned} \tag{27}$$

It is found from Eqs. (24) and (25) that

$$\begin{aligned}F_2(\zeta)=&\frac{b_z}{2\pi i}\left(\frac{\zeta}{\zeta-\zeta_0}-\frac{\zeta}{\zeta+R_2}\right)\\&-\frac{\mu_2-\mu_1+M}{\mu_1+\mu_2-M}\frac{b_z}{2\pi i}\left(\frac{\zeta}{\zeta-\zeta_1{}^*}-\frac{\zeta}{\zeta+\zeta_2{}^*}\right)\\&-\frac{\mu_2-\mu_1+M-N(k+1)}{\mu_1+\mu_2-M}\sum_{k=0}^{\infty}\overline{b_k}(k+1)\frac{R_1{}^{2k+2}}{\zeta^{k+1}}\\&+\frac{N(k+1)}{\mu_1+\mu_2-w_2}\sum_{k=0}^{\infty}a_k(k+1)\zeta^{-k-1}\\&+\frac{N}{\mu_1+\mu_2-M}\frac{b_z}{2\pi i}\left[\frac{\zeta_1{}^*\zeta}{(\zeta-\zeta_1{}^*)^2}+\frac{\zeta_2{}^*\zeta}{(\zeta+\zeta_2{}^*)^2}\right]\\&+\sum_{k=0}^{\infty}b_k(k+1)\zeta^{k+1}\end{aligned} \tag{28}$$

The displacement and stress boundary conditions in Eq. (7) can be rewritten as

$$[F_2(t)+F_3{}^*(t)]^{(2)}=[F_3(t)+F_2{}^{**}(t)]^{(3)},\ |t|=R_2 \tag{29}$$

$$[\mu_2F_2(t)-\mu_3F_3{}^*(t)]^{(2)}=[\mu_3F_3(t)-\mu_2F_2{}^{**}(t)]^{(3)},\ |t|=R_2 \tag{30}$$

Similarly, following the generalized Liouville theorem [35] and considering Eqs. (14), (16) and (17), the solutions of Eqs. (29) and (30) are explicitly obtained as

$$p(\zeta)=\begin{cases}F_2(\zeta)+F_3{}^*(\zeta),\ R_1<|\zeta|<R_2\\ F_3(\zeta)+F_2{}^{**}(\zeta),\ R_2<|\zeta|<\frac{R_2{}^2}{R_1}\end{cases} \tag{31}$$

$$q(\zeta)=\begin{cases}\mu_2F_2(\zeta)-\mu_3F_3{}^*(\zeta),\ R_1<|\zeta|<R_2\\ \mu_3F_3(\zeta)-\mu_2F_2{}^{**}(\zeta),\ R_2<|\zeta|<\frac{R_2{}^2}{R_1}\end{cases} \tag{32}$$

where

$$\begin{aligned}p(\zeta)=&\frac{b_z}{2\pi i}\left(\frac{\zeta}{\zeta-\zeta_0}-\frac{\zeta}{\zeta+R_2}\right)-\sum_{k=0}^{\infty}a_k(k+1)\zeta^{-k-1}\\&+\frac{b_z}{2\pi i}\left(\frac{\zeta}{\zeta-\zeta_2{}^{**}}-\frac{\zeta}{\zeta+R_2}\right)-\sum_{k=0}^{\infty}\overline{a_k}(k+1)\frac{\zeta^{k+1}}{R_2{}^{2k+2}}\end{aligned} \tag{33}$$

$$\begin{aligned}q(\zeta)=&\mu_2\frac{b_z}{2\pi i}\left(\frac{\zeta}{\zeta-\zeta_0}-\frac{\zeta}{\zeta+R_2}\right)-\mu_2\sum_{k=0}^{\infty}a_k(k+1)\zeta^{-k-1}\\&-\mu_2\frac{b_z}{2\pi i}\left(\frac{\zeta}{\zeta-\zeta_2{}^{**}}-\frac{\zeta}{\zeta+R_2}\right)\\&+\mu_2\sum_{k=0}^{\infty}\overline{a_k}(k+1)\frac{\zeta^{k+1}}{R_2{}^{2k+2}}+2\mu_3\frac{b_z}{2\pi i}\end{aligned} \tag{34}$$

Considering Eqs. (31)–(34), the analytical function $F_2(\zeta)$ is derived as

$$F_2(\zeta) = \frac{b_z}{2\pi i}\left(\frac{\zeta}{\zeta-\zeta_0} - \frac{\zeta}{\zeta+R_2}\right) - \sum_{k=0}^{\infty} a_k(k+1)\zeta^{-k-1} + \frac{2\mu_3}{\mu_2+\mu_3}\frac{b_z}{2\pi i} - \frac{\mu_2-\mu_3}{\mu_2+\mu_3}\frac{b_z}{2\pi i}\left(\frac{\zeta}{\zeta-\zeta_2^{**}} - \frac{\zeta}{\zeta+R_2}\right) + \frac{\mu_2-\mu_3}{\mu_2+\mu_3}\sum_{k=0}^{\infty}\overline{a_k}(k+1)\frac{\zeta^{k+1}}{R_2^{2k+2}} \tag{35}$$

In order to simultaneously satisfy all the boundary conditions on the interfaces Γ and Ω, the analytical function $F_2(\zeta)$ expressed by Eqs. (28) and (35) must be compatible to each other [30]. Physically, the compatibility conditions $F_2(\zeta)$ mean that the stress field and displacement field in the intermediate region ($R_1 < |\zeta| < R_2$) are unique. From Eqs. (28) and (35), the following equation is derived to deduce the undetermined coefficients a_k and b_k.

$$\begin{aligned}
&-\frac{\mu_2-\mu_1+M}{\mu_1+\mu_2-M}\frac{b_z}{2\pi i}\left(\frac{\zeta}{\zeta-\zeta_1^*} - \frac{\zeta}{\zeta+\zeta_2^*}\right) - \frac{\mu_2-\mu_1+M-N(k+1)}{\mu_1+\mu_2-M}\sum_{k=0}^{\infty}\overline{b_k}(k+1)\frac{R_1^{2k+2}}{\zeta^{k+1}} \\
&+\frac{N(k+1)}{\mu_1+\mu_2-M}\sum_{k=0}^{\infty}a_k(k+1)\zeta^{-k-1} \\
&+\frac{N}{\mu_1+\mu_2-M}\frac{b_z}{2\pi i}\left[\frac{\zeta_1^*\zeta}{(\zeta-\zeta_1^*)^2} + \frac{\zeta_2^*\zeta}{(\zeta+\zeta_2^*)^2}\right] \\
&+\sum_{k=0}^{\infty}b_k(k+1)\zeta^{k+1} = \frac{2\mu_3}{\mu_2+\mu_3}\frac{b_z}{2\pi i} \\
&-\frac{\mu_2-\mu_3}{\mu_2+\mu_3}\frac{b_z}{2\pi i}\left(\frac{\zeta}{\zeta-\zeta_2^{**}} - \frac{\zeta}{\zeta+R_2}\right) \\
&+\frac{\mu_2-\mu_3}{\mu_2+\mu_3}\sum_{k=0}^{\infty}\overline{a_k}(k+1)\frac{\zeta^{k+1}}{R_2^{2k+2}} - \sum_{k=0}^{\infty}a_k(k+1)\zeta^{-k-1}
\end{aligned} \tag{36}$$

Comparing the coefficients in the same power terms yields

$$\begin{aligned}
a_k = \frac{b_z}{2\pi i(k+1)}\Bigg\{&\frac{R_2^{2k+2}(\mu_2+\mu_3)[\mu_2-\mu_1+M-N(k+1)][\zeta_1^{*k+1} - (-\zeta_2^*)^{k+1}]}{(\mu_2+\mu_3)[\mu_1+\mu_2-M+N(k+1)]R_2^{2k+2} - (\mu_2-\mu_3)[\mu_2-\mu_1+M-N(k+1)]R_1^{2k+2}} \\
&+\frac{R_1^{2k+2}(\mu_2-\mu_3)[\mu_2-\mu_1+M-N(k+1)][R_2^{2k+2}/(-R_2)^{k+1} - R_2^{2k+2}/(\overline{\zeta_2^{**}})^{k+1}]}{(\mu_2+\mu_3)[\mu_1+\mu_2-M+N(k+1)]R_2^{2k+2} - (\mu_2-\mu_3)[\mu_2-\mu_1+M-N(k+1)]R_1^{2k+2}}\Bigg\}
\end{aligned} \tag{37}$$

$$\begin{aligned}
b_k = -\frac{b_z}{2\pi i(k+1)}\Bigg\{&\frac{(\mu_2-\mu_3)[\mu_2-\mu_1-M-N(k+1)][\overline{\zeta_1^*}^{k+1} - (-\overline{\zeta_2^*})^{k+1}]}{(\mu_2+\mu_3)[\mu_1+\mu_2+M+N(k+1)]R_2^{2k+2} - (\mu_2-\mu_3)[\mu_2-\mu_1-M-N(k+1)]R_1^{2k+2}} \\
&+\frac{(\mu_2-\mu_3)[\mu_1+\mu_2+M+N(k+1)][R_2^{2k+2}/(-R_2)^{k+1} - R_2^{2k+2}/(\zeta_2^{**})^{k+1}]}{(\mu_2+\mu_3)[\mu_1+\mu_2+M+N(k+1)]R_2^{2k+2} - (\mu_2-\mu_3)[\mu_2-\mu_1-M-N(k+1)]R_1^{2k+2}}\Bigg\}
\end{aligned} \tag{38}$$

By substituting Eqs. (37) and (38) into Eq. (14), the analytical expression of function $F_2(\zeta)$ is determined

$$F_2(\zeta) = \frac{b_z}{2\pi i}\left(\frac{\zeta}{\zeta-\zeta_0} - \frac{\zeta}{\zeta+R_2}\right) - \sum_{k=0}^{\infty}a_k(k+1)\zeta^{-k-1} + \sum_{k=0}^{\infty}b_k(k+1)\zeta^{k+1} \tag{39}$$

Finally, together with the relations of $f_k(\zeta) = \int[F_k(\zeta)/\zeta]d\zeta$ $(k = 1, 2, 3)$, the closed-form solutions of stress and displacement fields for a screw dislocation interacting with a circular nano-inhomogeneity near a bimaterial interface can be obtained from Eqs. (8) and (9). Here, the explicit expressions of complex potentials $f_1(\zeta)$, $f_2(\zeta)$ and $f_3(\zeta)$ are given as follows

$$\begin{aligned}
f_1(\zeta) = &\frac{2\mu_2}{\mu_1+\mu_2+M}\frac{b_z}{2\pi i}[\ln(\zeta-\zeta_0) - \ln(\zeta+R_2)] - \frac{N}{\mu_1+\mu_2+M}\frac{b_z}{2\pi i}\left(\frac{\zeta_0}{\zeta-\zeta_0} + \frac{R_2}{\zeta+R_2}\right) \\
&-\frac{N}{\mu_1+\mu_2+M}\sum_{k=0}^{\infty}\overline{a_k}(k+1)\frac{\zeta^{k+1}}{R_1^{2k+2}} - \frac{N}{\mu_1+\mu_2+M} \\
&\times\sum_{k=0}^{\infty}b_k(k+1)\zeta^{k+1} + \frac{2\mu_2}{\mu_1+\mu_2+M}\sum_{k=0}^{\infty}b_k\zeta^{k+1}
\end{aligned} \tag{40}$$

$$f_2(\zeta) = \frac{b_z}{2\pi i}[\ln(\zeta-\zeta_0) - \ln(\zeta+R_2)] + \sum_{k=0}^{\infty}a_k\zeta^{-k-1} + \sum_{k=0}^{\infty}b_k\zeta^{k+1} \tag{41}$$

$$f_3(\zeta) = \frac{2\mu_3}{\mu_2+\mu_3}\frac{b_z}{2\pi i}\ln\zeta + \frac{2\mu_2}{\mu_2+\mu_3}\frac{b_z}{2\pi i}[\ln(\zeta-\zeta_0) - \ln(\zeta+R_2)] + \frac{2\mu_2}{\mu_2+\mu_3}\sum_{k=0}^{\infty}a_k\zeta^{-k-1} \tag{42}$$

In order to validate the analytical results derived in this paper, the reduced results are given. When the interface stresses vanish ($\mu^\Gamma = \tau^\Gamma = 0$), the solutions shown in Eqs. (40)–(42) can be reduced to

$$f_1(\zeta) = \frac{2\mu_2}{\mu_1+\mu_2}\frac{b_z}{2\pi i}[\ln(\zeta-\zeta_0) - \ln(\zeta+R_2)] + \frac{2\mu_2}{\mu_1+\mu_2}\sum_{k=0}^{\infty}b_k\zeta^{k+1} \tag{43}$$

$$f_2(\zeta) = \frac{b_z}{2\pi i}[\ln(\zeta-\zeta_0) - \ln(\zeta+R_2)] + \sum_{k=0}^{\infty}a_k\zeta^{-k-1} + \sum_{k=0}^{\infty}b_k\zeta^{k+1} \tag{44}$$

$$f_3(\zeta) = \frac{2\mu_3}{\mu_2+\mu_3}\frac{b_z}{2\pi i}\ln\zeta + \frac{2\mu_2}{\mu_2+\mu_3}\frac{b_z}{2\pi i}[\ln(\zeta-\zeta_0) - \ln(\zeta+R_2)] + \frac{2\mu_2}{\mu_2+\mu_3}\sum_{k=0}^{\infty}a_k\zeta^{-k-1} \tag{45}$$

where

$$\begin{aligned}
a_k = &\frac{b_z}{2\pi i(k+1)} \\
&\times\Bigg\{\frac{R_2^{2k+2}(\mu_2+\mu_3)(\mu_2-\mu_1)[\zeta_1^{*k+1} - (-\zeta_2^*)^{k+1}]}{(\mu_2+\mu_3)(\mu_1+\mu_2)R_2^{2k+2} - (\mu_2-\mu_3)(\mu_2-\mu_1)R_1^{2k+2}} \\
&+\frac{R_1^{2k+2}(\mu_2-\mu_3)(\mu_2-\mu_1)[R_2^{2k+2}/(-R_2)^{k+1} - R_2^{2k+2}/(\overline{\zeta_2^{**}})^{k+1}]}{(\mu_2+\mu_3)(\mu_1+\mu_2)R_2^{2k+2} - (\mu_2-\mu_3)(\mu_2-\mu_1)R_1^{2k+2}}\Bigg\}
\end{aligned}$$

and

$$b_k = -\frac{b_z}{2\pi i(k+1)}$$
$$\times\left\{\frac{(\mu_2-\mu_3)(\mu_2-\mu_1)[\overline{\zeta_1{}^*}^{k+1}-(-\overline{\zeta_2{}^*})^{k+1}]}{(\mu_2+\mu_3)(\mu_1+\mu_2){R_2}^{2k+2}-(\mu_2-\mu_3)(\mu_2-\mu_1){R_1}^{2k+2}}\right.$$
$$\left.+\frac{(\mu_2-\mu_3)(\mu_1+\mu_2)[{R_2}^{2k+2}/(-R_2)^{k+1}-{R_2}^{2k+2}/(\zeta_2{}^{**})^{k+1}]}{(\mu_2+\mu_3)(\mu_1+\mu_2){R_2}^{2k+2}-(\mu_2-\mu_3)(\mu_2-\mu_1){R_1}^{2k+2}}\right\}$$

As expected, the solutions of complex potentials $f_j(\zeta)$ are in agreement with the results by Chai et al. [33] for the case of coupling interaction between a screw dislocation and a circular inclusion with a bimaterial interface. In addition, if we take $\mu_3=0$, the new solutions are similar to the case derived by Li [25] for the interaction between a screw dislocation and a circular nano-inclusion in the half-plane model. The current reduced solutions are presented as follows

$$\begin{aligned}f_1(\zeta) = {}& \frac{2\mu_2}{\mu_1+\mu_2+M}\frac{b_z}{2\pi i}[\ln(\zeta-\zeta_0)-\ln(\zeta+R_2)] \\ & -\frac{N}{\mu_1+\mu_2+M}\frac{b_z}{2\pi i}\left(\frac{\zeta_0}{\zeta-\zeta_0}+\frac{R_2}{\zeta+R_2}\right) \\ & -\frac{N}{\mu_1+\mu_2+M}\sum_{k=0}^{\infty}\overline{a_k}(k+1)\frac{\zeta^{k+1}}{{R_1}^{2k+2}}-\frac{N}{\mu_1+\mu_2+M} \\ & \times\sum_{k=0}^{\infty}b_k(k+1)\zeta^{k+1}+\frac{2\mu_2}{\mu_1+\mu_2+M}\sum_{k=0}^{\infty}b_k\zeta^{k+1}\end{aligned} \tag{46}$$

$$f_2(\zeta) = \frac{b_z}{2\pi i}[\ln(\zeta-\zeta_0)-\ln(\zeta+R_2)]+\sum_{k=0}^{\infty}a_k\zeta^{-k-1}+\sum_{k=0}^{\infty}b_k\zeta^{k+1} \tag{47}$$

where

$$a_k = \frac{b_z}{2\pi i(k+1)}\times\left\{\frac{{R_2}^{2k+2}[\mu_2-\mu_1+M-N(k+1)][{\zeta_1{}^*}^{k+1}-(-\zeta_2{}^*)^{k+1}]}{[\mu_1+\mu_2-M+N(k+1)]{R_2}^{2k+2}-[\mu_2-\mu_1+M-N(k+1)]{R_1}^{2k+2}}\right.$$
$$\left.+\frac{{R_1}^{2k+2}[\mu_2-\mu_1+M-N(k+1)][{R_2}^{2k+2}/(-R_2)^{k+1}-{R_2}^{2k+2}/(\overline{\zeta_2{}^{**}})^{k+1}]}{[\mu_1+\mu_2-M+N(k+1)]{R_2}^{2k+2}-[\mu_2-\mu_1+M-N(k+1)]{R_1}^{2k+2}}\right\}$$

and

$$b_k = -\frac{b_z}{2\pi i(k+1)}\times\left\{\frac{[\mu_2-\mu_1-M-N(k+1)][\overline{\zeta_1{}^*}^{k+1}-(-\overline{\zeta_2{}^*})^{k+1}]}{[\mu_1+\mu_2+M+N(k+1)]{R_2}^{2k+2}-[\mu_2-\mu_1-M-N(k+1)]{R_1}^{2k+2}}\right.$$
$$\left.+\frac{[\mu_1+\mu_2+M+N(k+1)][{R_2}^{2k+2}/(-R_2)^{k+1}-{R_2}^{2k+2}/(\zeta_2{}^{**})^{k+1}]}{[\mu_1+\mu_2+M+N(k+1)]{R_2}^{2k+2}-[\mu_2-\mu_1-M-N(k+1)]{R_1}^{2k+2}}\right\}$$

2.2. *A screw dislocation in Material 3*

Letting a screw dislocation with Burgers vector b_z lie at point z_0 in Material 3, the complex function vectors can be written as:

$$f_1(z) = f_{10}(z),\ z\in S_1 \tag{48}$$

$$f_2(z) = f_{20}(z),\ z\in S_2 \tag{49}$$

$$f_3(z) = \frac{b_z}{2\pi i}\ln(z-z_0)+f_{30}(z),\ z\in S_3 \tag{50}$$

where the complex function vectors $f_{10}(z)$, $f_{20}(z)$ and $f_{30}(z)$ are holomorphic in the regions where they are defined, respectively.

By noting Eq. (1), Eqs. (48)–(50) can lead to

$$f_1(\zeta) = f_{10}(\zeta),\ \zeta\in S_1' \tag{51}$$

$$f_2(\zeta) = \sum_{k=0}^{\infty}c_k\zeta^{-k-1}+\sum_{k=0}^{\infty}d_k\zeta^{k+1},\ \zeta\in S_2' \tag{52}$$

$$f_3(\zeta) = \frac{b_z}{2\pi i}[\ln(\zeta-\zeta_0)-\ln(\zeta+R_2)]+f_{30}(\zeta),\ \zeta\in S_3' \tag{53}$$

Referring to Eqs. (14)–(16), the following complex function vectors can be written as

$$\begin{aligned}F_2(\zeta) = {}& \zeta f_2'(\zeta) = -\sum_{k=0}^{\infty}c_k(k+1)\zeta^{-k-1} \\ & +\sum_{k=0}^{\infty}d_k(k+1)\zeta^{k+1},\ R_1<|\zeta|<R_2\end{aligned} \tag{54}$$

$$\begin{aligned}{F_2}^*(\zeta) = {}& \overline{F_2}({R_1}^2/\zeta) = -\sum_{k=0}^{\infty}\overline{c_k}(k+1)\frac{\zeta^{k+1}}{{R_1}^{2k+2}} \\ & +\sum_{k=0}^{\infty}\overline{d_k}(k+1)\frac{{R_1}^{2k+2}}{\zeta^{k+1}},\quad \frac{{R_1}^2}{R_2}<|\zeta|<R_1\end{aligned} \tag{55}$$

$$\begin{aligned}{F_2}^{**}(\zeta) = {}& \overline{F_2}({R_2}^2/\zeta) = -\sum_{k=0}^{\infty}\overline{c_k}(k+1)\frac{\zeta^{k+1}}{{R_2}^{2k+2}} \\ & +\sum_{k=0}^{\infty}\overline{d_k}(k+1)\frac{{R_2}^{2k+2}}{\zeta^{k+1}},\quad R_2<|\zeta|<\frac{{R_2}^2}{R_1}\end{aligned} \tag{56}$$

$${F_3}^*(\zeta) = \overline{F_3}({R_2}^2/\zeta) = \frac{b_z}{2\pi i}\left(\frac{\zeta}{\zeta-\zeta_2{}^{**}}-\frac{\zeta}{\zeta+R_2}\right)+{F_{30}}^*(\zeta),\ |\zeta|<R_2 \tag{57}$$

Using the similar method in Section 2.1, the relations of the complex potentials $F_1(\zeta)$ and $F_3(\zeta)$ can be obtained

$$\begin{aligned}F_1(\zeta) = {}& \frac{2\mu_2-N(k+1)}{\mu_1+\mu_2+M}\sum_{k=0}^{\infty}d_k(k+1)\zeta^{k+1} \\ & -\frac{N(k+1)}{\mu_1+\mu_2+M}\sum_{k=0}^{\infty}\overline{c_k}(k+1)\frac{\zeta^{k+1}}{{R_1}^{2k+2}}\end{aligned} \tag{58}$$

$$\begin{aligned}F_3(\zeta) = {}& \frac{b_z}{2\pi i}\left(\frac{\zeta}{\zeta-\zeta_0}-\frac{\zeta}{\zeta+R_2}\right) \\ & +\frac{\mu_2-\mu_3}{\mu_2+\mu_3}\frac{b_z}{2\pi i}\left(\frac{\zeta}{\zeta-\zeta_2{}^{**}}-\frac{\zeta}{\zeta+R_2}\right) \\ & -\frac{2\mu_2}{\mu_2+\mu_3}\sum_{k=0}^{\infty}a_k(k+1)\zeta^{-k-1}\end{aligned} \tag{59}$$

The complex potential $f_2(\zeta)$ is determined by the following equation

$$-\sum_{k=0}^{\infty}a_k(k+1)\zeta^{-k-1}+\frac{\mu_2-\mu_3}{\mu_2+\mu_3}\sum_{k=0}^{\infty}\overline{a_k}(k+1)\frac{\zeta^{k+1}}{{R_2}^{2k+2}}$$
$$+\frac{2\mu_3}{\mu_2+\mu_3}\frac{b_z}{2\pi i}\left(\frac{\zeta}{\zeta-\zeta_0}-\frac{\zeta}{\zeta+R_2}\right)$$

$$= \sum_{k=0}^{\infty} b_k(k+1)\zeta^{k+1} - \frac{\mu_2-\mu_1+M-N(k+1)}{\mu_1+\mu_2-M}\sum_{k=0}^{\infty}\overline{b_k}(k+1)\frac{R_1{}^{2k+2}}{\zeta^{k+1}} + \frac{N(k+1)}{\mu_1+\mu_2-M}\sum_{k=0}^{\infty}a_k(k+1)\frac{1}{\zeta^{k+1}} \tag{60}$$

Comparing the coefficients of the same power terms in Eq. (60) yields

$$c_k = \frac{b_z}{2\pi i(k+1)} \times \frac{2\mu_3[\mu_2-\mu_1+M-N(k+1)][R_2{}^{2k+2}/\overline{\zeta_0}^{k+1} - R_2{}^{2k+2}/(-R_2)^{k+1}]R_1{}^{2k+2}}{(\mu_2+\mu_3)[\mu_1+\mu_2-M+N(k+1)]R_2{}^{2k+2} - (\mu_2-\mu_3)[\mu_2-\mu_1+M-N(k+1)]R_1{}^{2k+2}} \tag{61}$$

$$d_k = \frac{b_z}{2\pi i(k+1)} \times \frac{-2\mu_3[\mu_1+\mu_2+M+N(k+1)][R_2{}^{2k+2}/\zeta_0{}^{k+1} - R_2{}^{2k+2}/(-R_2)^{k+1}]}{(\mu_2+\mu_3)[\mu_1+\mu_2+M+N(k+1)]R_2{}^{2k+2} - (\mu_2-\mu_3)[\mu_2-\mu_1-M-N(k+1)]R_1{}^{2k+2}} \tag{62}$$

Now the complex function vectors $f_1(\zeta), f_2(\zeta)$ and $f_3(\zeta)$ can be obtained using Eqs. (51)–(62).

$$f_1(\zeta) = \frac{2\mu_2-N(k+1)}{\mu_1+\mu_2+M}\sum_{k=0}^{\infty}d_k\zeta^{k+1} - \frac{N(k+1)}{\mu_1+\mu_2+M}\sum_{k=0}^{\infty}\overline{c_k}\frac{\zeta^{k+1}}{R_1{}^{2k+2}} \tag{63}$$

$$f_2(\zeta) = \sum_{k=0}^{\infty}c_k\zeta^{-k-1} + \sum_{k=0}^{\infty}d_k\zeta^{k+1} \tag{64}$$

$$f_3(\zeta) = \frac{b_z}{2\pi i}[\ln(\zeta-\zeta_0) - \ln(\zeta+R_2)] + \frac{\mu_2-\mu_3}{\mu_2+\mu_3}\frac{b_z}{2\pi i} \times [\ln(\zeta-\zeta_2{}^{**}) - \ln(\zeta+R_2)] + \frac{2\mu_2}{\mu_2+\mu_3}\sum_{k=0}^{\infty}c_k\zeta^{-k-1} \tag{65}$$

It is worth pointing out that from Eqs. (63)–(65), when $\mu_1=0$, $\mu_2=\mu_3$, and the distance h between the center of inclusion and the bimaterial interface approaches infinity, the solutions of complex potentials are in line with the results of Fang and Liu [20] for the case of size-dependent elastic interaction between a screw dislocation and a circular nano-hole with surface stress, and the reduced results are written as follows

$$f(\zeta) = \frac{b_z}{2\pi i}\ln(\zeta-\zeta_0) + \sum_{k=0}^{\infty}c_k\zeta^{-k-1} \tag{66}$$

where $\mu_2=\mu_3=\mu$, $f(\zeta)=f_2(\zeta)=f_3(\zeta)$ and $c_k = \frac{b_z}{2\pi i(k+1)}\frac{\mu-(\mu^\Gamma-\tau^\Gamma)(k+1)}{\mu+(\mu^\Gamma-\tau^\Gamma)(k+1)}\left(\frac{R^2}{\overline{\zeta_0}}\right)^{k+1}$

3. Image forces on screw dislocations

The image forces exerted on dislocations will be evaluated in this section, which is of primary importance in analyzing the physical and mechanical behaviors in mobility and the so-called trapping mechanism of dislocations. Associated with the Peach–Koehler formula [30,41], the image force acting on a screw dislocation at point z_0 can be expressed as

$$f_x - if_y = ib_z[\tau^*_{xz2}(z_0) - i\tau^*_{yz2}(z_0)] \tag{67}$$

where f_x and f_y are the force components in the x-axis and y-axis directions, respectively, and τ^*_{xz2} and τ^*_{yz2} denote the perturbation stress components at the dislocation point, which can be derived by subtracting those attributions to the dislocation in the corresponding infinite homogeneous medium from the stresses obtained currently.

Table 1 – Material constants for typical metals [44,45].

	Al	Cu	Ni	α-Fe	W
μ (GPa)	28	33	95	85	160
b_z (nm)	0.286	0.256	0.249	0.248	0.274

By noting Eq. (9), we have

$$\tau^*_{xz}(z_0) - i\tau^*_{yz}(z_0) = \mu\left.\frac{f'(\zeta)}{\omega'(\zeta)}\right|_{\zeta=\zeta_0} \tag{68}$$

Referring to the work of Lee [42], the explicit expression of the image force acting on the screw dislocation for the present problem can be written as

$$f_x - if_y = \frac{ib_z\mu_2(\zeta+R_2)^2}{R_2{}^2-R_1{}^2}\left[-\sum_{k=0}^{\infty}a_k(k+1)\zeta^{-k-2} + \sum_{k=0}^{\infty}b_k(k+1)\zeta^k\right] \tag{69}$$

for the dislocation in Material 2, and

$$f_x - if_y = \frac{ib_z\mu_3(\zeta+R_2)^2}{R_2{}^2-R_1{}^2}\left[\frac{\mu_2-\mu_3}{\mu_2+\mu_3}\frac{b_z}{2\pi i}\left(\frac{1}{\zeta-\zeta_2{}^{**}} - \frac{1}{\zeta+R_2}\right) - \frac{2\mu_2}{\mu_2+\mu_3}\sum_{k=0}^{\infty}c_k(k+1)\zeta^{-k-2}\right] \tag{70}$$

for the dislocation in Material 3.

4. Numerical examples and discussion

Having the expressions of the image forces given in Eqs. (69) and (70), the influence of various parameters (the material elastic mismatch, the interface stress, the distance between the center of inclusion and the bimaterial interface, and the location of the screw dislocation) upon image force acting on the screw dislocation can be well calculated. In subsequent numerical calculation, the relative shear moduli are defined as $\alpha=\mu_1/\mu_2$ and $\beta=\mu_3/\mu_2$, and the intrinsic length $\gamma=(\mu^\Gamma-\tau^\Gamma)/\mu_2$ [23,43]. Former studies have shown that μ^Γ and τ^Γ are on the order of 1 N/m and their values can be positive or negative depending upon the crystallographic orientation [8]. According to the results of Miller and Shenoy [8], the absolute value of the intrinsic length $\gamma=(\mu^\Gamma-\tau^\Gamma)/\mu_2$ is nearly 0.1 nm. In addition, the magnitude of Burgers vector b_z is not constant but depends on the specific materials. The material constants of Material 2 are taken from metal Cu ($\mu_2=33$ GPa, $b_z=0.256$ nm) listed in Table 1.

In this section, we will just focus on the case that a screw dislocation is located in Material 2 in detail, and the case in Material 3 is omitted to save space. Supposing that the screw dislocation lies at point x_0 on the x-axis ($R_1 < x_0 < R_2$), in this case, $f_y=0$ and the component of normalized image force along the x-axis direction is defined as $f_{x0}=2\pi f_x/(\mu_2 b_z{}^2)$. In Figs. 2–5, we illustrate the variation of the values of f_{x0} with

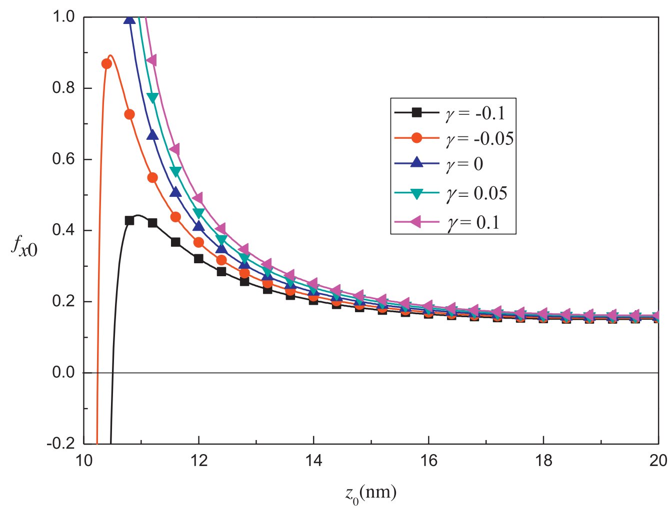

Fig. 2 – Normalized force f_{x0} versus z_0 for $\alpha = 1.2$, $\beta = 0.8$, $R_1 = 10$ nm and $h = 10$ nm.

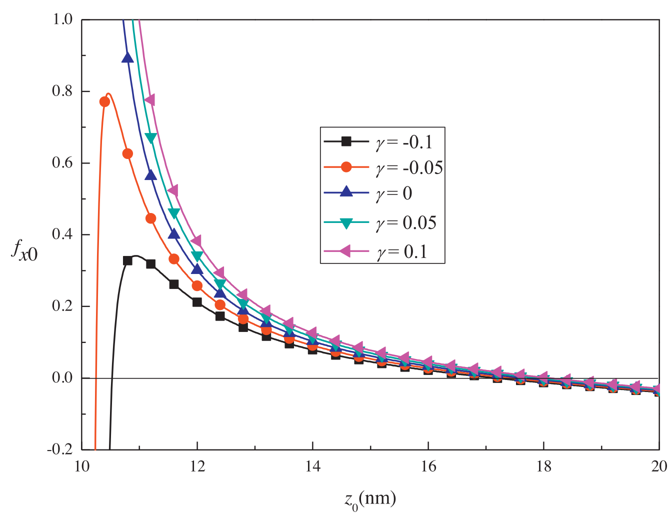

Fig. 3 – Normalized force f_{x0} versus z_0 for $\alpha = 1.2$, $\beta = 1.2$, $R_1 = 10$ nm and $h = 10$ nm.

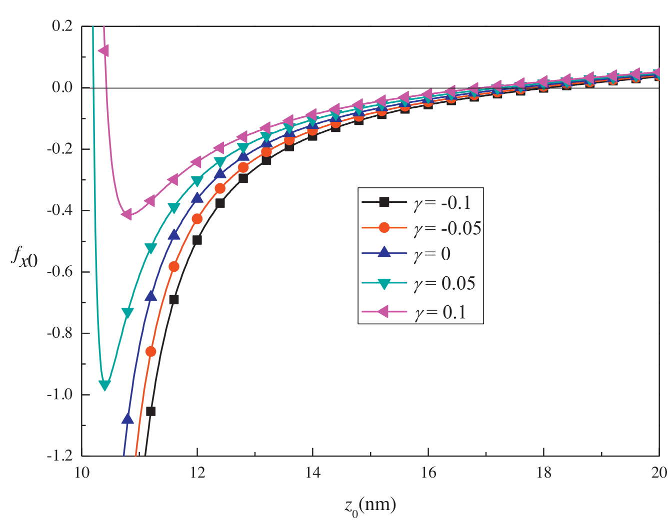

Fig. 4 – Normalized force f_{x0} versus z_0 for $\alpha = 0.8$, $\beta = 0.8$, $R_1 = 10$ nm and $h = 10$ nm.

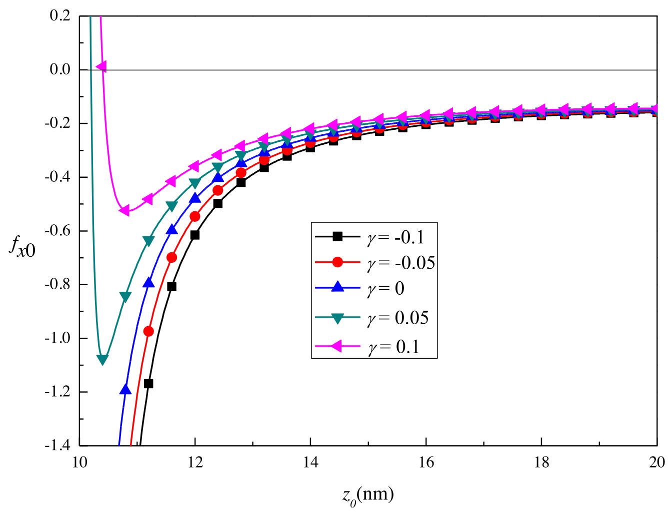

Fig. 5 – Normalized force f_{x0} versus z_0 for $\alpha = 0.8$, $\beta = 1.2$, $R_1 = 10$ nm and $h = 10$ nm.

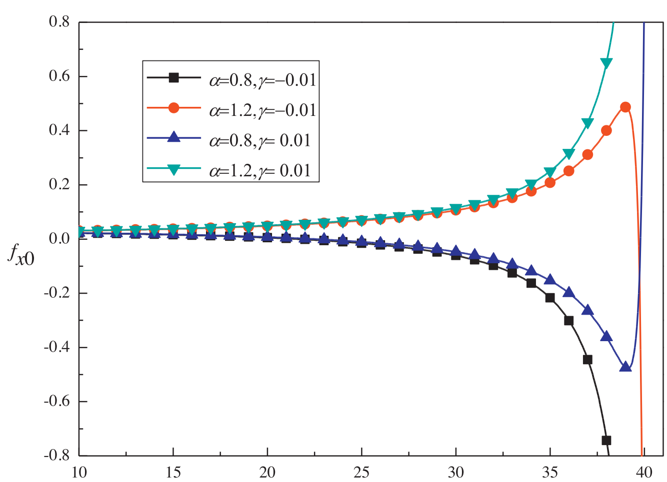

Fig. 6 – Normalized force f_{x0} versus R_1 with $\beta = 0.8$, $z_0 = 41$ nm, $h = 50$ nm for different α, γ.

respect to parameter z_0 for the selected material constants and the intrinsic length γ ($R_1 = 10$ nm, $h = 10$ nm). It is shown from Figs. 2–5 that, if the interface stresses are positive, with the increase of γ, the screw dislocation will be repelled more strongly by the inclusion (Material 1), and there may be zero ($\beta = 0.8$), or a stable equilibrium position point ($\beta = 1.2$) in Material 2 when the matrix (Material 2) is softer than the inclusion; while if the interface stresses are negative, the screw dislocation will be first attracted then repelled by the inclusion, and there may be a non-stable ($\beta = 0.8$), or a stable equilibrium position point ($\beta = 1.2$) in Material 2. At the same time, if the interface stresses are negative, the screw dislocation will be attracted toward the inclusion, and there may be zero ($\beta = 1.2$), or a non-stable equilibrium position ($\beta = 0.8$) when the matrix is stiffer than the inclusion; while the positive interface stresses are likely to give rise to a non-stable ($\beta = 1.2$), or a stable equilibrium position point ($\beta = 0.8$) in Material 2. The same as those shown by Fang and his groups [18,29,30,37], the mechanical behavior of interface effect revealed in this study shows that the dislocation can be attracted by the negative interface stresses and repelled by the positive interface stresses, which differs from the classical cases under the same conditions that the screw dislocation can be attracted by the stiffer matrix or repelled by the softer matrix when the dislocation approaches the nano-inclusion. Comparing with the solution [25] for a screw dislocation and a nano-inclusion in the half-plane with the classical solution [33] ($\gamma = 0$), it is observed that more equilibrium positions of the dislocation may be available when the dislocation is near the nanoscale inclusion and is close to the bimaterial interface, respectively. On the other hand, the image force exerted on the dislocation may be more complicated than in the half-plane case which is dependent on the attraction of half-plane to the screw dislocation.

The variation of normalized image force f_{x0} versus parameter R_1 is depicted in Fig. 6 with the selected material constants of $h = 50$ nm, $\beta = 0.8$, $z_0 = 41$ nm, and different relative shear moduli and intrinsic lengths. Fig. 6 shows that, with the increase of R_1, the screw dislocation will first be slightly affected by the relative shear modulus and then be increasingly influenced by the interface stress.

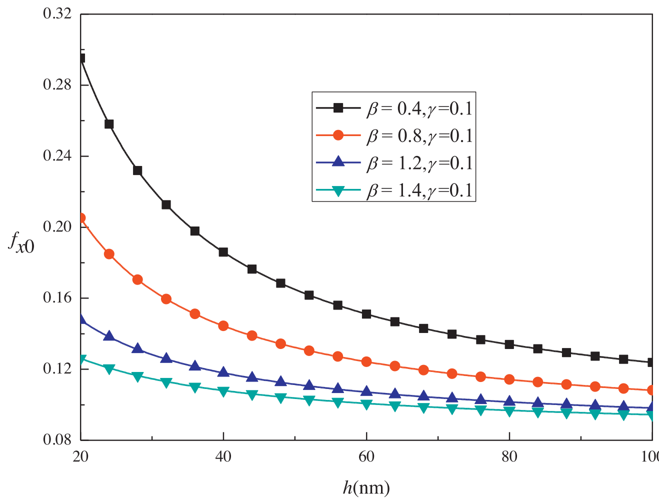

Fig. 7 – Normalized force f_{x0} versus h with $\alpha = 1.2$, $\gamma = 0.1$ nm, $z_0 = 15$ nm, $R_1 = 10$ nm for different β.

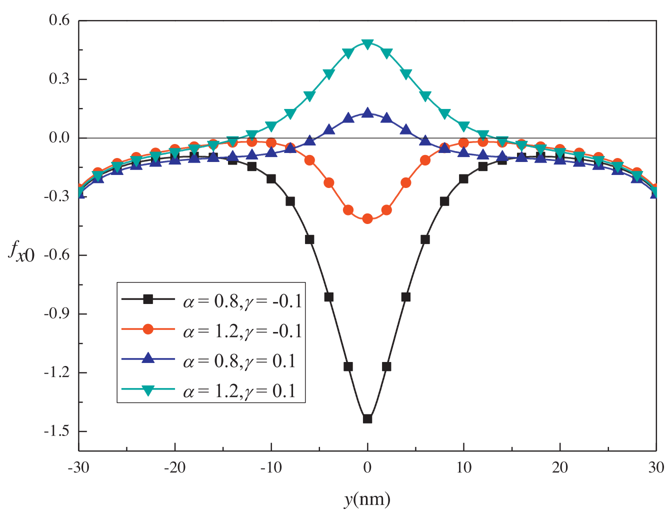

Fig. 8 – Normalized force f_{x0} versus y with $x = 13$ nm, $\beta = 1.2$, $R_1 = 10$ nm, $h = 10$ nm for different α, γ.

The variation of normalized image force f_{x0} versus parameter h is depicted in Fig. 7 with the selected material constants of $\gamma = 0.1$ nm, $R_1 = 10$ nm, $z_0 = 43$ nm and different relative shear moduli. Fig. 7 indicates that, with the increase of h, the normalized image force acting on the screw dislocation will decrease slowly and reach the critical value, which is closely related to the relative shear modulus β.

The variation of normalized image forces f_{x0} and f_{y0} ($f_{y0} = 2\pi f_y/(\mu_2 b_z{}^2)$) versus parameter z_0 is depicted in Figs. 8 and 9 with the selected material constants of $\beta = 1.2$, $R_1 = 10$ nm, $h = 10$ nm and different relative shear moduli and intrinsic lengths when the dislocation is located at the straight line $x = 13$ nm. In Fig. 8, it can be seen that the normalized image force f_{x0} acting on the screw dislocation is axisymmetric about the x-axis, and the screw dislocation will be repelled by Material 3 when the dislocation is located away from the x-axis. Especially, the repellent force or attractive force exerted on the dislocation reaches maximum when the dislocation lies on the x-axis. Fig. 9 demonstrates that, the normalized image force f_{y0} acting on the screw dislocation is the center of symmetry at point (0, 0), and the negative interface stress shows a stronger impact on the image force f_{y0} than the positive interface stress. Comparing with the solution to the problem with a screw dislocation and a nano-inclusion in the half-plane, we can observe that the equilibrium positions of the dislocation only exist on the x-axis, when the dislocation is close to the inclusion with interface effect.

5. Conclusions

A study on the elastic interaction between a screw dislocation and a circular nano-inclusion near a bimaterial interface is carried out. The stress boundary condition at the interface between the nano-inhomogeneity and the matrix is modified by incorporating the surface/interface stress. The solution to the problem is derived analytically by combining the complex variable method of Muskhelishvili, the conformal mapping function and Laurent series expansion techniques. The image force and the equilibrium position of a screw

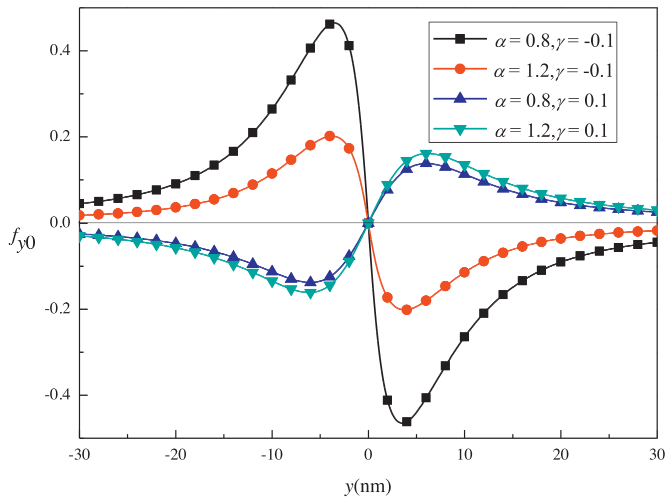

Fig. 9 – Normalized force f_{y0} versus y with $x = 13$ nm, $\beta = 1.2$, $R_1 = 10$ nm, $h = 10$ nm for different α, γ.

dislocation near a bimaterial interface are presented by numerical calculations and discussed in detail. It is found that the dislocation can be attracted by the negative interface tresses, and repelled by the positive interface stresses, which is due to the local hardening/softening on interfaces; while the classical solutions are that the screw dislocation can be attracted by the softer matrix or rejected by the harder matrix when the dislocation is near the inclusion. In fact, the stability of the dislocations is closely linked to plastic deformations of nanocrystalline materials. Therefore, ultra-fine second phase particles involving nano-inhomogeneity are often introduced for improving the strengthening and hardening properties of nanomaterials such as alloys and composites. On the other hand, when the inclusion and Material 3 are both stiffer than the matrix ($\mu_1 > \mu_2$ and $\mu_3 > \mu_2$), a new stable equilibrium position for the screw dislocation in the matrix appears near the bimaterial interface. When the inclusion and Material 3 are both softer than the matrix ($\mu_1 < \mu_2$ and $\mu_3 < \mu_2$), a new unstable equilibrium position can exist close to the bimaterial interface. Furthermore, in certain situations, there is always a new stable or unstable equilibrium position of dislocation near the nanoscale inclusion depending on different material combinations.

REFERENCES

[1] P. Bose, N. Paitya, S. Bhattacharya, et al., Influence of light waves on the effective electron mass in quantum wells, wires, inversion layers and superlattices, Quantum Matter 1 (2) (2012) 89–126.

[2] Z.Y. Ou, S.D. Pang, A screw dislocation interacting with a coated nano-inhomogeneity incorporating interface stress, Mater. Sci. Eng. A 528 (6) (2011) 2762–2775.

[3] X.-Q. Fang, X.-H. Wang, L.-L. Zhang, Interface effect on the dynamic stress around an elliptical nano-inhomogeneity subjected to anti-plane shear waves, Comput. Mater. Continua 16 (3) (2010) 229–246.

[4] I. Ovid'ko, N Skiba, Nanotwins induced by grain boundary deformation processes in nanomaterials, Scripta Mater 71 (2014) 33–36.

[5] S.R. Kalehbasti, M.Y. Gutkin, H Shodja, Wedge disclinations in the shell of a core–shell nanowire within the surface/interface elasticity, Mech. Mater 68 (2014) 45–63.

[6] J. Li, Q. Fang, Y. Liu, Interface effects on elastic behavior of a screw dislocation around double nanowires, Physica B: Cond. Matter 442 (2014) 6–11.

[7] W. Zhao, N. Tao, J. Guo, et al., High density nano-scale twins in Cu induced by dynamic plastic deformation, Scripta Mater 53 (6) (2005) 745–749.

[8] R.E. Miller, V.B. Shenoy, Size-dependent elastic properties of nanosized structural elements, Nanotechnology 11 (3) (2000) 139.

[9] M.E. Gurtin, A.I. Murdoch, A continuum theory of elastic material surfaces, Arch. Ration. Mech. Anal. 57 (4) (1975) 291–323.

[10] M. Gurtin, J. Weissmller, F. Larche, A general theory of curved deformable interfaces in solids at equilibrium, Philos. Mag. A 78 (5) (1998) 1093–1109.

[11] H. Ahmadzadeh-Bakhshayesh, M.Y. Gutkin, H. Shodja, Surface/interface effects on elastic behavior of a screw dislocation in an eccentric core–shell nanowire, Int. J. Solids Struct. 49 (13) (2012) 1665–1675.

[12] P. Sharma, S. Ganti, Size-dependent Eshelby's tensor for embedded nano-inclusions incorporating surface/interface energies, J. Appl. Mech. 71 (5) (2004) 663–671.

[13] H. Duan, J. Wang, Z. Huang, et al., Size-dependent effective elastic constants of solids containing nano-inhomogeneities with interface stress, J. Mech. Phys. Solids 53 (7) (2005) 1574–1596.

[14] C. Lim, Z. Li, L. He, Size dependent, non-uniform elastic field inside a nano-scale spherical inclusion due to interface stress, Int. J. Solids Struct. 43 (17) (2006) 5055–5065.

[15] T. Chen, G.J. Dvorak, Fibrous nanocomposites with interface stress: Hill's and Levin's connections for effective moduli, Appl. Phys. Lett. 88 (21) (2006) 211912.

[16] L. Tian, R. Rajapakse, Analytical solution for size-dependent elastic field of a nanoscale circular inhomogeneity, J. Appl. Mech. 74 (3) (2007) 568–574.

[17] P. Sharma, L. Wheeler, Size-dependent elastic state of ellipsoidal nano-inclusions incorporating surface/interface tension, J. Appl. Mech. 74 (3) (2007) 447–454.

[18] Q. Fang, Y. Liu, Size-dependent elastic interaction of a screw dislocation with a circular nano-inhomogeneity incorporating interface stress, Scripta Mater 55 (1) (2006) 99–102.

[19] Y. Liu, Q. Fang, Analysis of a screw dislocation inside an inhomogeneity with interface stress, Mater. Sci. Eng. A 464 (1) (2007) 117–123.
[20] Q. Fang, Y. Liu, Size-dependent elastic interaction between a screw dislocation and a circular nano-hole with surface stress, Phys. Status Solidi (b) 243 (4) (2006) R28–R30.
[21] M.Y. Gutkin, S.R. Kalehbasti, H. Shodja, Surface/interface effects on elastic behavior of an edge dislocation in the shell of a core–shell nanowire, Eur. J. Mech. A/Solids 41 (2013) 86–100.
[22] L. Tian, R. Rajapakse, Elastic field of an isotropic matrix with a nanoscale elliptical inhomogeneity, Int. J. Solids Struct. 44 (24) (2007) 7988–8005.
[23] J. Luo, Z. Xiao, Analysis of a screw dislocation interacting with an elliptical nano inhomogeneity, Int. J. Eng. Sci. 47 (9) (2009) 883–893.
[24] J. Luo, X. Wang, On the anti-plane shear of an elliptic nano inhomogeneity, Eur. J. Mech. A/Solids 28 (5) (2009) 926–934.
[25] J. Li, X. Zeng, Y. Liu, Screw dislocation interacting with a nanoscale cylindrical inclusion in an elastic half-plane, J. Comput. Theor. Nanos 10 (11) (2013) 2714–2721.
[26] R. Christensen, K. Lo, Solutions for effective shear properties in three phase sphere and cylinder models, J. Mech. Phys. Solids 27 (4) (1979) 315–330.
[27] H.A. Luo, Y. Chen, An edge dislocation in a three-phase composite cylinder model, J. Appl. Mech. 58 (1991) 75–86.
[28] Z. Xiao, B. Chen, A screw dislocation interacting with inclusions in fiber-reinforced composites, Acta Mech. 155 (3-4) (2002) 203–214.
[29] H. Feng, Q. Fang, Y. Liu, et al., Image force and stability of a screw dislocation inside a coated cylindrical inhomogeneity with interface stresses, Acta Mech. 220 (1-4) (2011) 315–329.
[30] Q. Fang, Y. Liu, P. Wen, Screw dislocations in a three-phase composite cylinder model with interface stress, J. Appl. Mech. 75 (4) (2008) 041019.
[31] Z. Xiao, B. Chen, A screw dislocation interacting with a coated fiber, Mech. Mater. 32 (8) (2000) 485–494.
[32] Q. Fang, Y. Liu, B. Jin, et al., Effect of interface stresses on the image force and stability of an edge dislocation inside a nanoscale cylindrical inclusion, Int. J. Solids Struct. 46 (6) (2009) 1413–1422.
[33] H. Chai, C. Jiang, F. Song, et al., The coupling interaction of a screw dislocation with a bimaterial interface and a nearby circular inclusion, Arch. Appl. Mech. 85 (11) (2015) 1733–1742.
[34] C. Jiang, H. Chai, P. Yan, et al., The interaction of a screw dislocation with a circular inhomogeneity near the free surface, Arch. Appl. Mech. 84 (3) (2014) 343–353.
[35] N.I. Muskhelishvili, Some Basic Problems of the Mathematical Theory of Elasticity, Springer Science & Business Media, 1977.
[36] Z. Ou, S. Pang, A screw dislocation interacting with a coated nano-inhomogeneity incorporating interface stress, Mater. Sci. Eng. A 528 (6) (2011) 2762–2775.
[37] Q.H. Fang, Y.W. Liu, B. Jin, et al., Interaction between a dislocation and a core–shell nanowire with interface effects, Int. J. Solids Struct. 46 (46) (2009) 1539–1546.
[38] E. Smith, The interaction between dislocations and inhomogeneities—I, Int. J. Eng. Sci. 6 (3) (1968) 129–143.
[39] Y. Liu, Q. Fang, C. Jiang, A piezoelectric screw dislocation interacting with an interphase layer between a circular inclusion and the matrix, Int. J. Solids Struct. 41 (11) (2004) 3255–3274.
[40] A.H. England, Complex Variable Methods in Elasticity, Courier Corporation, 2012.
[41] J. Shi, Z. Li, An approximate solution of the interaction between an edge dislocation and an inclusion of arbitrary shape, Mech. Res. Commun. 33 (6) (2006) 804–810.
[42] S. Lee, The image force on the screw dislocation around a crack of finite size, Eng. Fract. Mech. 27 (5) (1987) 539–545.
[43] H.M. Shodja, M.Y. Gutkin, S.S. Moeini-Ardakani, Effect of surface stresses on elastic behavior of a screw dislocation inside the wall of a nanotube, Phys. Status Solidi (b) 248 (6) (2011) 1437–1441.
[44] V. Gryaznov, I. Polonsky, A. Romanov, et al., Size effects of dislocation stability in nanocrystals, Phys. Rev. B 44 (1) (1991) 42.
[45] V. Gryaznov, A. Kaprelov, A. Romanov, Size effect of dislocation stability in small particles and microcrystallites, Scripta Metall. 23 (8) (1989) 1443–1448.